World Electric Vehicle Journal

MDPI

Article

Simulation and Testing of Self-Reconfigurable Battery Advanced Functions for Automotive Application

Rémy Thomas [1], Nicolas Léto [2], Jérome Lachaize [2], Sylvain Bacquet [3,*], Yan Lopez [1] and Leandro Cassarino [4]

[1] CEA, Liten, Université Grenoble Alpes, F-38000 Grenoble, France; remy.thomas@cea.fr (R.T.); yan.lopez@cea.fr (Y.L.)
[2] Vitesco Technologies, 40 Avenue du Général de Croutte, 31100 Toulouse, France; nicolas.leto@vitesco.com (N.L.); jerome.lachaize@vitesco.com (J.L.)
[3] CEA, Leti, Université Grenoble Alpes, F-38000 Grenoble, France
[4] CEA, CEA Tech Nouvelle Aquitaine, F-33600 Pessac, France; leandro.cassarino@cea.fr
* Correspondence: sylvain.bacquet@cea.fr

Abstract: This article presents the design and production work carried out jointly by Vitesco Technologies and the CEA in order to build a Self-Reconfigurable Battery (SRB) demonstrator representative of an electric vehicle traction battery pack. The literature demonstrates that the use of an SRB allows for individual bypassing or serialization of each cell in a battery pack, enabling control of the voltage output and dynamic balancing of the battery pack during all phases of vehicle use. The simulations and tests presented in this article confirm that the use of an SRB results in a 6% reduction in energy consumption compared to a Conventional Battery Pack (CBP) on a driving profile based on WLTP cycles. Additionally, an SRB enhances fast charging performance, with a charging time that is 22% faster than a CBP. Furthermore, it is shown that an SRB without a voltage inversion capability can still be connected directly to the AC grid for charging without the need for a dedicated converter, using only a single diode bridge rectifier for the whole system.

Keywords: battery management system; electric vehicle (EV); fast charge; self-reconfigurable battery

check for updates

Citation: Thomas, R.; Léto, N.; Lachaize, J.; Bacquet, S.; Lopez, Y.; Cassarino, L. Simulation and Testing of Self-Reconfigurable Battery Advanced Functions for Automotive Application. *World Electr. Veh. J.* **2024**, *15*, 250. https://doi.org/10.3390/wevj15060250

Academic Editor: Peter Van den Bossche

Received: 15 March 2024
Revised: 21 May 2024
Accepted: 23 May 2024
Published: 8 June 2024

Copyright: © 2024 by the authors. Licensee MDPI, Basel, Switzerland. This article is an open access article distributed under the terms and conditions of the Creative Commons Attribution (CC BY) license (https://creativecommons.org/licenses/by/4.0/).

1. Introduction

As shown in many articles [1], battery-switching technologies of Self-Reconfigurable Batteries (SRBs) promise significant improvements in terms of autonomy and battery life, cell balancing [2–7], recharging capacity [8–11], improving the efficiency of vehicle drive trains [12–14] and even cell aging [15–17]. Their operating principle is as follows: switches are added to the power paths linking the cells to enable the number of active stages in series and parallel to be modulated dynamically [18], depending on the type of SRB. Some systems even incorporate H-bridges to enable the generation of alternating voltages, opening the way to motor control without an inverter [19–21] and direct recharging on the AC grid without a charger [10,22,23]. However, the increase in the number of switches raises the question of safety impact [24–27].

The aim of this study is to highlight the benefits of a simplified and cost-effective SRB architecture adapted from the design presented in [28]. The benefits include improved motor inverter efficiency, reduced charging time for DC fast charging and AC charging on the electricity grid.

In this study, fulfilling Vitesco Technologies requirements, the SRB architecture dynamically generates a strictly positive DC voltage to optimize the efficiency of the motor's inverter. It also allows the absorption of a rectified AC current to enable the battery to be charged from an AC voltage source without a charger, by means of a simple rectifier. Hence, only the dynamic modulation of the number of series stages is implemented. To maintain the capability of recharging on the AC grid, a simple rectifier diode bridge is added at the

head of the architecture instead of H-bridges on cells, as it is not necessary to generate a sinusoidal waveform when discharging.

To assess the benefits, a Conventional Battery Pack (CBP) and the SRB system are compared by simulation in a complete simulation environment incorporating the various components of an electric vehicle power train. In addition, these simulations are validated on a real demonstrator. The comparison is based on different use cases. The first use case is a battery discharge following a driving profile based on cycles from the Worldwide harmonized Light vehicles Test Procedure (WLTP). Different batches of cells are used such as new and aged cells with 5% to 10% loss of State Of Health (SoH) in order to introduce dispersion conditions representative of an aged vehicle pack [29]. It is therefore possible to study the benefits of SRBs using an end-of-life battery pack or even a second-life battery pack. A comparison is then made using a fast charging use case to assess the benefits in terms of stored energy and charging time.

Finally, a direct charging experiment using a rectified AC current from the AC grid is presented to demonstrate the possibility of charging directly from the AC grid without an intermediate converter, despite the absence of the voltage inversion capability in the SRB architecture implemented.

The SRB demonstrator developed by Vitesco Technologies and the French Alternative Energies and Atomic Energy Commission (CEA) integrates a maximum of 120 cells in series with a maximum current of 125 A for charging and discharging. The system consists of a main controller that communicates with 20 modules. These modules are connected to each other in series in the power path. Each module independently controls the switching of six cells, each of which can be dynamically connected in series or bypassed. The system is flexible, making it easy to add or remove modules in series to adjust the maximum voltage. Initially, the system is composed of 14 Ah NMC cells. Then, in a second phase, 90 Ah cells are used. The total number of modules used is adjusted to match the number of cells available for each batch of cells. This setup makes it possible to validate the operation of cell switching in an electric vehicle application.

This article is an expansion of the work presented in EVS36 [30] with additional experimentations based on the introduction of a fourth batch of cells from a used BMW-i3 battery pack that has traveled 25,000 km. The different geometry of these cells meant that the demonstrator had to be modified. The driving profiles also had to be adapted to the new cell capacities. This expansion made it possible to present the results of an SRB system integrating cells directly representative of a real battery pack in use and resulting from a large-scale industrial process, which is unprecedented in the state of the art of reconfigurable battery packs.

2. Simulation

The main objectives are to demonstrate the benefits of the different capabilities listed in the introduction to this paper, by comparing the proposed SRB solution with equivalent CBP. With regard to optimizing the efficiency of the motor inverter, it is necessary to consider an SRB capable of supplying the necessary voltage up to the end-of-discharge conditions of the system. Thus, compared with a CBP for a given segment, the equivalent SRB to be considered must be made up of a larger number of cells in series. Lower-capacity cells are then required to maintain the relevance of the comparison from an energetic point of view. A process of adaptation is therefore necessary. This is why different battery configurations are simulated, in an environment representative of electric vehicles, to carry out the comparison.

The two batteries are dimensioned in order to provide the same energy at the wheel at the beginning of life, taking into account a capacity dispersion of 2% within the cells. In this simulation, the reference CBP is a 96S3P battery with 60 Ah cells, while the SRB has a 144S2P architecture with the same 60 Ah cells. To reduce the cost of this technology, a grouping of cells in series is also considered: instead of having one cell for each bypass switch/serial switch entity, groups of four cells in series for each bypass switch/serial

switch entity are used. Consequently, the SRB in this simulation has 36 groups with each group consisting of four 1S2P cells and one bypass switch/serial switch entity.

2.1. Driving Simulation

The simulation environment representative of electric vehicles is described in detail in a previous study [31], where it was used to compare balancing solutions during driving cycles. For this study, the simulation model is improved by the use of representative energetic cells based on actual parameters as well as a representative dispersion of the cells in the pack.

Figure 1 highlights the benefits, in terms of driven distance, of the aged SRB compared with the aged CBP. The comparison is made based on a capacity reduced to 70% of the nominal capacity and a capacity dispersion of 4.8%. The cumulated losses in the battery pack are detailed for the SRB values, while the values in brackets correspond to the difference SRB minus CBP. Due to the control DC link voltage capability, one can see that a better global powertrain efficiency is achieved with a reduction of 51 Wh per 100 km. This increased efficiency and the SRB's ability to manage the dispersal of capacity result in a 6% (+24 km) increase in range, which is of the same order of magnitude as the gains seen in [13].

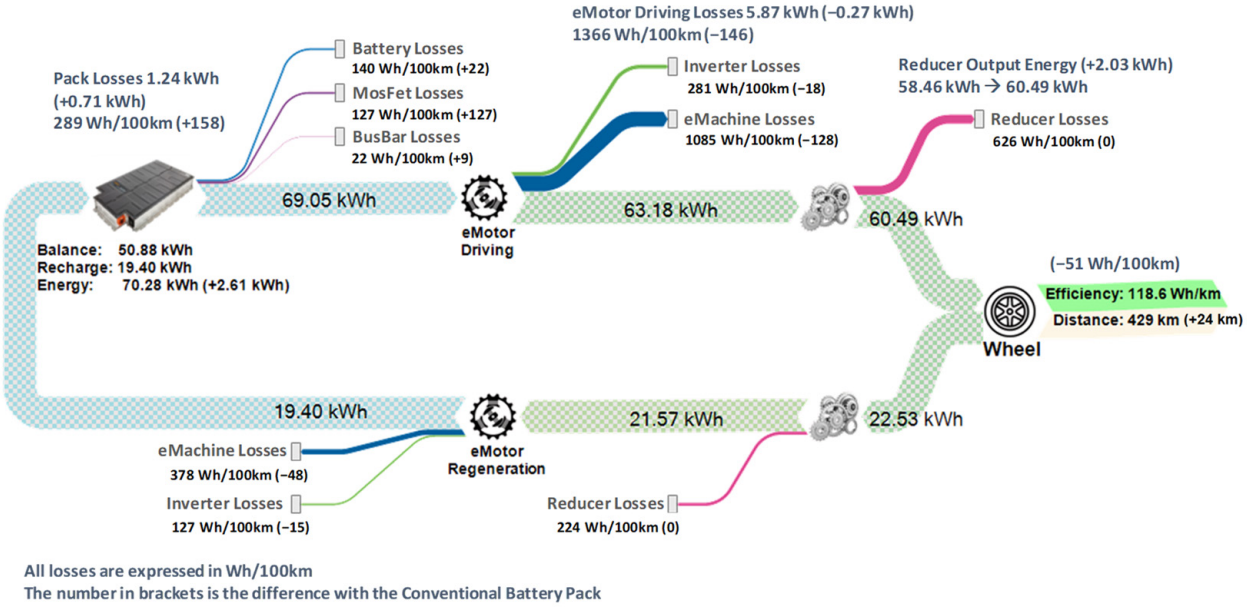

Figure 1. Sankey diagram for SRB/CBP comparison—driving use case.

2.2. Fast Charging Simulation

The CBP and SRB system configurations used for the previous driving profile are this time used to simulate 130 kW DC fast charging. This time, the nominal capacities are used to compare the solutions at the beginning of their lifetime. With regard to the SRB configuration defined above, the voltage set point of the DC bus output is fixed to 450 V. To take better account of the constraints of fast charging, the simulation model is updated with an improved thermal representativeness.

Figure 2 illustrates this comparison. By convention, the charging current and power are positive, as they are considered from the charger point of view. The power curves show that the maximum charge power can be maintained for a much longer time with the SRB system than with the CBP system. This is due to the faster rise in cell temperature in the CBP configuration, which leads to the limitation of the charging current.

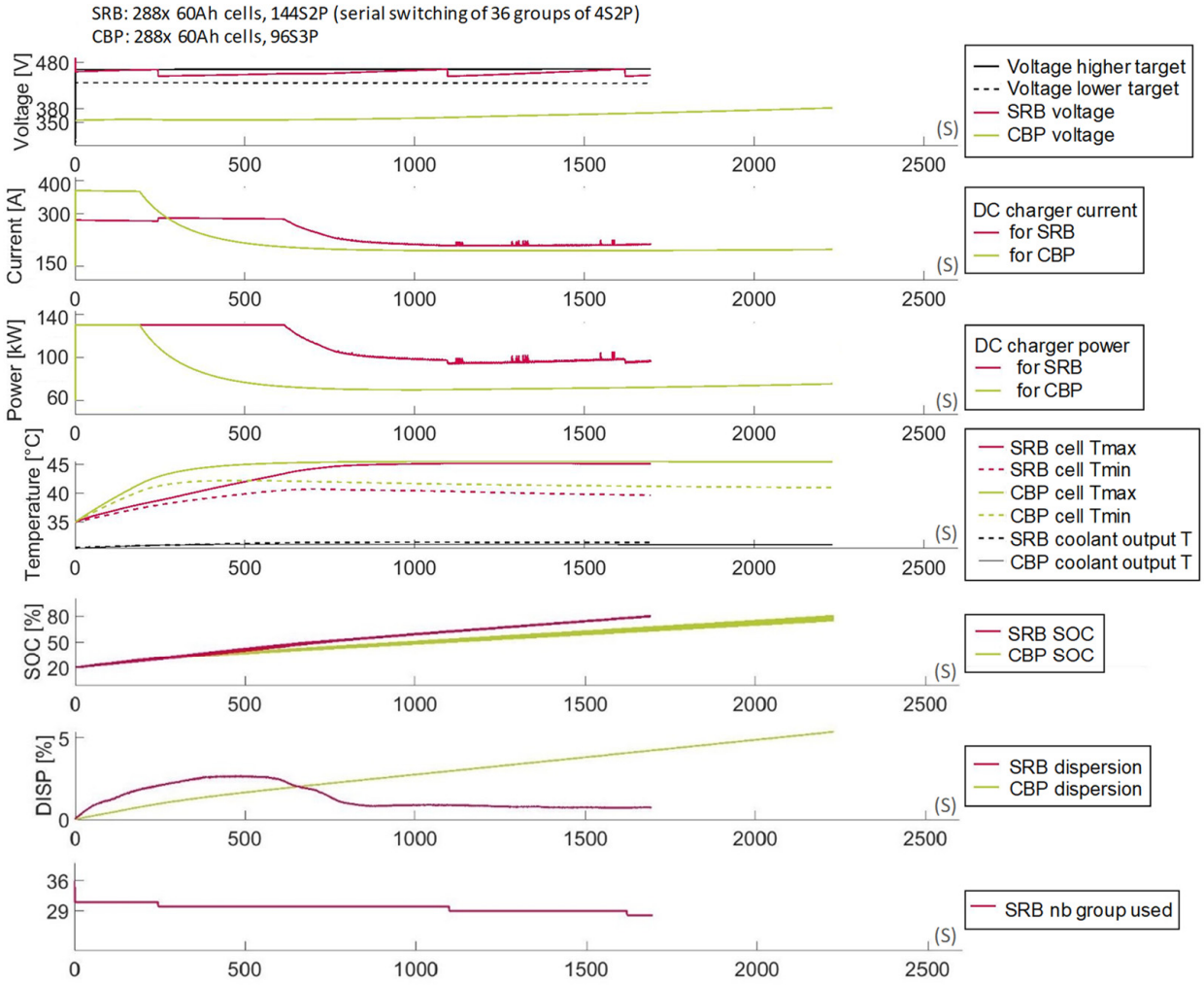

Figure 2. Simulation of fast DC charging for CBP and SRB.

At the beginning of the charge, almost all of the SRB cells are set in serial to reach the DC link voltage set point. Consequently, the cell-to-cell dispersion within the SRB is higher than the CBP's one when the charging power remains high. Nevertheless, when the charging power decreases, a smaller number of cells is required in serial. Then, power cell balancing is possible again, resulting in a very low cell-to-cell dispersion. This illustrates the great effectiveness of SRB power cell balancing.

Table 1 highlights the energies and losses involved in fast charging for both CBP and SRB. The losses are increased by 40% in the SRB compared to the CBP because of the additional electronic components and the higher recharging power allowed. Assuming identical charger efficiency, the DC charging efficiencies are, respectively, 97.0% and 98.2% for SRB and CBP. However, despite this increase in losses, the charging time from 20% to 80% state of charge is reduced from 37 min (2234 s) to 28 min (1687 s) due to the reduction in current required to charge the battery, which delays the rise in cell temperature. Charging time is therefore 24% faster with the SRB based on a battery capable of undergoing the same WLTP test than with the CPB configuration. This reduced fast charging time is a key element in the competitive BEV market [32]. In addition, the maximum current required from the charger is reduced.

Table 1. Energies and losses for fast DC charging.

	Battery Chemical Energy [kWh]	Battery Losses [kWh]	MosFet Losses [kWh]	BusBar Losses [kWh]	Battery Energy [kWh]
CBP	−50.20	0.80	0.00	0.12	−51.11
SRB	−50.19	0.83	0.60	0.10	−51.72

3. Experimental System Overview

The experimental system is an adaptation of the presented system in [28]. It consists of one master and twenty modules, each composed of 6 switchable cells. The modules provide voltage and temperature measurements through an isolated RS485 bus to the master. The master controller measures the overall voltage and current, processes the cell voltage and temperature measurements received from the modules and sends back the switching orders to be applied. In addition, this master controller includes high-level application management capabilities such as battery pack voltage regulation, dynamic cell balancing and safety features. Dynamic cell balancing is performed by alternating the cells used on the power path in order to manage the current drawn on each cell to provide the output power [33]. The state of charge of each series level is assessed by coulomb counting using a single current sensor located at the battery pack, combined with information on the bypass or series states of each level. For the test carried out in this study, the global amount of energy exchanged when operating WLTP cycles, or during the fast charging test, is assessed using the current sensor of the power lab equipment of the climatic chamber.

The architecture of the experimental SRB is illustrated in Figure 3. Unlike many reconfigurable batteries that rely on a phase-shifting carrier, this implementation uses a true real-time process to control the output voltage while using low-cost local controllers. This enables a faulty cell to be removed and replaced by the master controller in less than 100 µs from the time it is detected. It also allows the shape of a signal such as a disturbed electrical grid to be tracked as closely as possible, thereby reducing the size of the filtering components. In the case of DC discharge and DC fast charge, switch SW1 is closed and switch SW2 is open. For AC charging, switch SW1 is open and switch SW2 is closed to connect the SRB to the electrical grid via a rectifier diode bridge. The SRB then generates a rectified signal adjusted in real time to follow the waveform of the rectifier bridge with a slightly lower amplitude to create a charging current flowing through the cells. The internal global current sensor is used to control the current exchanged by adjusting the voltage differences between the SRB and the output of the rectifier diode bridge.

The CBP and SRB are compared using, for both cases, the self-reconfigurable electrical architecture, in order to use the same experimental setup. Hence, by serializing all the cells, the demonstrator behaves like a CBP, where all the cells of the batch are serialized without possible modification, while the SRB can control its output voltage by bypassing some cells. As the first cell in each module is used to power the switching electronics, the related serial levels are constantly bypassed from the power path to avoid interference in the comparison between SRB and CBP, in end-of-charge or end-of-discharge conditions and in the energy balance.

To charge and discharge the system, a secure test chamber with an 800 V 400 A power supply serving as both a source and sink is employed. Figure 4 shows the test bench setup in operation inside the test chamber. The experimental comparison enables the results obtained by simulation to be verified.

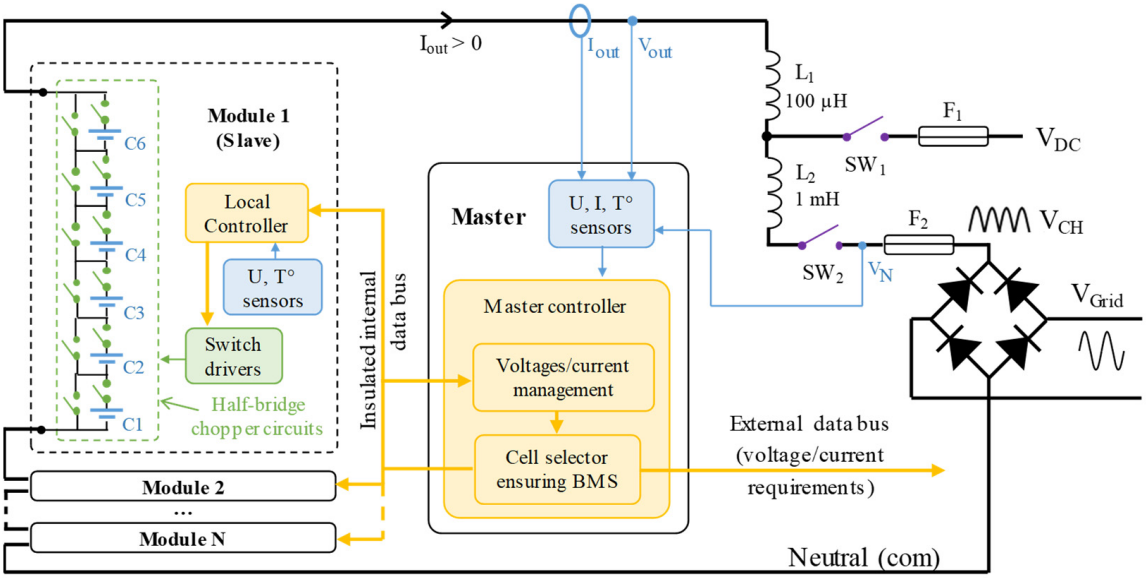

Figure 3. Experimental Self-Reconfigurable Battery architecture.

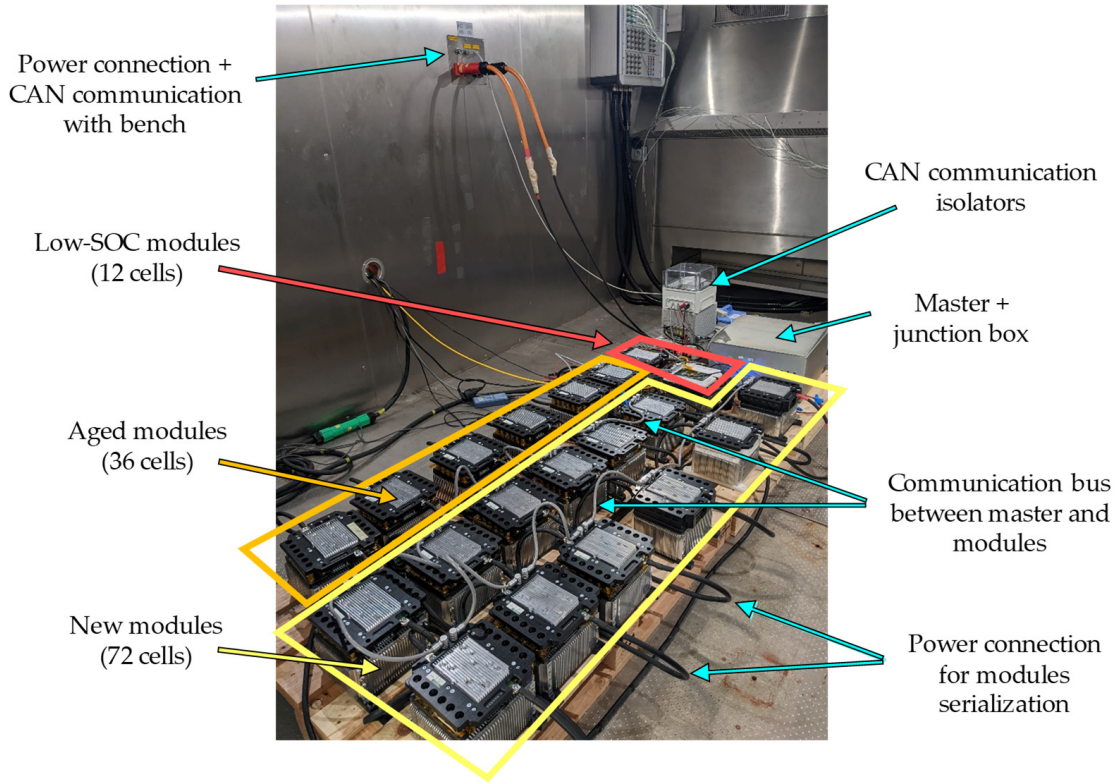

Figure 4. Self-Reconfigurable Battery test bench, 120 serial cells subdivided in 20 modules of 6 serial cells.

4. Experimental Comparisons with a Driving Profile Based on the Worldwide Harmonized Test Cycles for Light Vehicles (WLTC)

In the case of discharge comparisons over a driving cycle, one of the main objectives is to demonstrate the feasibility of optimizing inverter efficiency with a real SRB system. To this end, the inverter model is considered reliable and the simulation of its efficiency is used to generate the power profiles applied to the experimental configurations as well as the battery voltage set point profile for the SRB. The aim of the experiment is then to verify that the SRB is indeed capable of responding to the dynamic profiles of the voltage

set point and that the gain in autonomy compared with a real CBP corresponds to those observed in the simulation. Additionally, another objective of the experiment is to compare the behavior of a CBP (in which cells cannot be bypassed) and that of an SRB with regard to cell-to-cell dispersion. Indeed, cell-to-cell dispersion has a significant impact on the performance of electric vehicles [34–36]. The comparison is carried out during a discharge imposed by a driving profile, which consists of several consecutive WLTCs.

Four batches of cells are created to address different use case scenarios. For each comparison, the same batch is used in both the CBP and the SRB. The first batch comprises 72 new NMC 14 Ah CALB cells. The second batch consists of 36 NMC 14 Ah CALB cells artificially aged by a laboratory cycling process. The aging process was carried out individually for each cell and therefore does not incorporate the aging divergence phenomenon that can be observed in a Conventional Battery Pack. The third batch is made of 36 cells from a mix of new NMC 14 Ah CALB cells and new NMC 14 Ah CALB cells slightly discharged to give a lower initial capacity. This batch is used to emulate a second life scenario using cells from different States Of Health (SOHs). The fourth batch is made of 42 NMC 94 Ah SDI cells from a real BMW i3 battery pack of around 25,000 km, in order to assess the benefits associated with the characteristics of the cells in a real commercial battery pack. A first batch of 60 new cells, a second and third batch of 30 cells and a fourth batch of 35 cells are finally used for comparison, considering that the first cell of each module is permanently bypassed from the power path. The characteristics of the different batches are summarized in Table 2.

Table 2. Batch characteristics.

Cell Batch ID	Use Case	Cell Details	Nb of Cells	Nb of Modules	Nb of Cells Used for Comparison
1	Beginning of life	New NMC 14 Ah (CALB)	72	12	60
2	Aged cells	Artificially aged NMC 14 Ah (CALB)	36	6	30
3	Second life	Mix of full and partially discharged NMC 14 Ah (CALB)	36	6	30
4	Cells with a lifetime of around 25,000 real-life km	BMW-i3 NMC 94 Ah (SDI)	42	7	35

To assess the dispersions involved in the experimental comparisons, cell capacities are estimated by coulomb counting with a specific charge and discharge cycle at a rate of 0.1 C between a minimum voltage of 3 V and a maximum voltage of 4.18 V. A dispersion of 0.95% for batch 1 of the new cells is observed, which remains realistic compared with what can be classically assessed for other cell references in the literature [37]. The dispersion of artificially aged cells in batch 2 is of the same order at 1.1%, which is quite low for cells representative of an aged pack [38]. This can be explained by the use of an individual aging process rather than a group process as in a Conventional Battery Pack where discrepancies can be observed with the increase in the number of cycles. The capacities of cells constituting batches 1 and 2 are, respectively, presented in Figure 5a,b, while the capacities of the cells in batches 3 and 4 are shown in Sections 4.3 and 4.4. The distinctive colors of each cell serve to enhance contrast during reading and have no other significance.

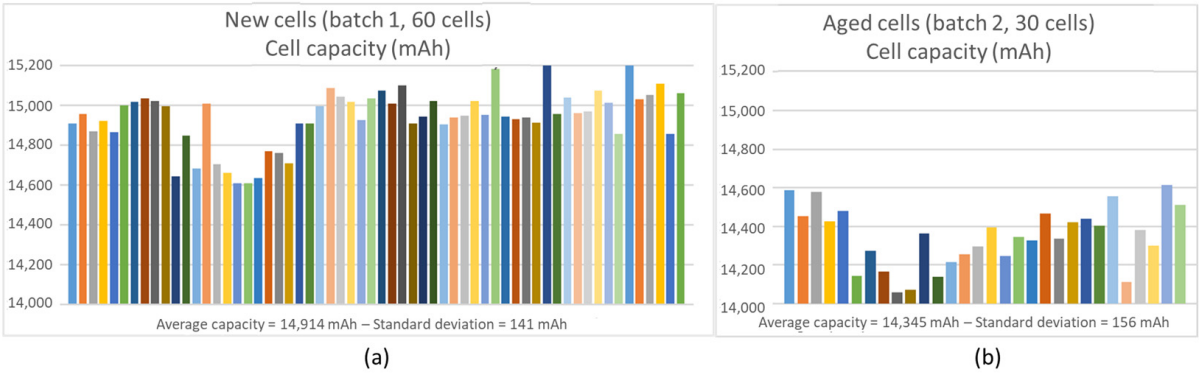

Figure 5. Capacity of cells constituting (**a**) batch 1 and (**b**) batch 2. Colors only to improve contrast.

The power profile generated from the simulation corresponds to the power consumed at the wheel. It takes into account the number of cells included in each batch to provide the corresponding power set point to be applied to the CBP and SRB packs. The optimum voltage set point for SRB tests is also generated for each batch according to the number of cells to be used.

Unlike the CBP, the SRB has the ability to balance the cells during charge and discharge. As the cells are always balanced, the SRB allows all the energy to be extracted from all the cells in the pack. In a CBP, this is not possible because the pack discharge must stop when a cell reaches its lower voltage limit, even if other cells still have energy. To ensure a fair comparison between CBP and SRB, all cells are fully charged and properly balanced before each test. All cells start at 4.18 V, and the test stops at the end of the driving profile or when the first of the cells under consideration reaches 3 V.

4.1. Driving Profile with New Cells (Batch 1)

Figure 6 shows the result of the driving profile with new cells (batch 1) in the SRB (top) and CBP (bottom) configurations. On the SRB profile, the battery output voltage set point (in orange) is perfectly stable at around 125 V, with the exception of two slots of around 200 s at times 1540 s and 3320 s, where the set point voltage changes dynamically to follow the parts of the WTLP cycle where power requirements are greater. The SRB voltage measurement (in blue) shows that the battery is perfectly in line with the set voltage, even during the most dynamic periods of the WLTP cycle, demonstrating the SRB's ability to generate the voltage profile required to optimize the inverter's efficiency in various driving phases. This optimization enables the SRB to complete the entire driving profile, unlike the CBP, which stops prematurely at 4364 s because a cell reaches the low voltage limit of 3 V.

Over a discharge period of 4364 s, which marks the end of the CBP's discharge, the SRB discharged 2886 Wh, while the CBP discharged 3060 Wh. The SRB therefore consumed 5.7% less energy than the CBP for the same distance traveled. The fact that the observed difference in consumption corresponds to the difference predicted by the simulation shows that the power profiles imposed are consistent with the simulation. At the end of the CBP driving profile, we observed that the cells were not well balanced, with a VCellMax–VCellMin difference of 180 mV, due to the dispersion of the cells' capacity in batch 1. In contrast, the SRB was able to balance the cells at all times, resulting in a VCellMax–VCellMin difference of less than 5 mV at the end of the driving profile. The figures of this test are reported in Table 3.

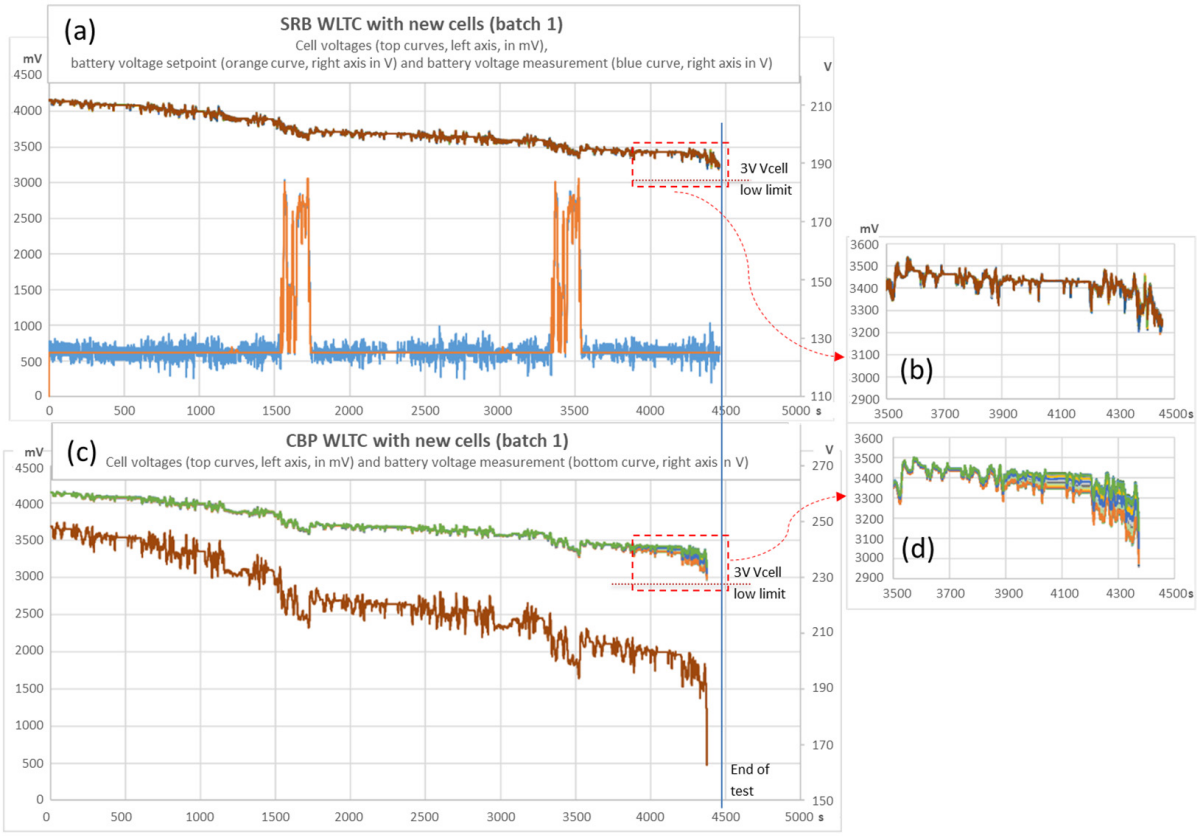

Figure 6. Driving profile with new cells (batch 1): (**a**) SRB configuration results; (**b**) zoom on SRB configuration results; (**c**) CBP configuration results; (**d**) zoom on CBP configuration results. Cell voltages colors only to improve contrast.

Table 3. Figures of WLTC test with new cells (batch 1).

	CBP	**SRB**
Run time	4364 s	4458 s
Remaining energy at end of cycle	0 Wh	104 Wh
Cell balance at end of cycle	Δ = 180 mV	Δ < 5 mV
Discharged–charged energies	@4364 s: 3060 Wh (batt low)	@4364 s: 2886 Wh @4455 s (end cycle): 2981 Wh (104 Wh left)

4.2. Driving Profile with Artificially Aged Cells (Batch 2)

Figure 7 shows the result of the driving profile with aged cells (batch 2) with the SRB (top) and CBP (bottom) configurations. The power profiles and the SRB set point profile are updated to take into account the reduction in the number of available cells compared to the first batch discharge experiment. The cells in batch 2 exhibited a lower average capacity, which resulted in neither the CBP nor the SRB configuration reaching the end of the test.

During a discharge period of 4027 s, the SRB discharged 1388 Wh while the CBP discharged 1468 Wh. The SRB consumed 5.45% less energy than the CBP for the same period, which once again shows that the power profiles applied are consistent with the simulation. The 1.1% capacity dispersion of artificially aged cells is not sufficient to introduce an additional gain in favor of the SRB, especially if the end of the CBP and SRB discharge occurs in a moderate power section of the WLTP cycle. Nevertheless, it can be observed that the emergence of cell voltage dispersion in the CBP occurs concurrently with the end of the second high-power phase of the WLTP cycle at 3500 s. The cell voltage imbalance of the CBP is also increased, as shown in Figure 7d. This suggests that a slightly

greater dispersion in cell capacity could have had a greater impact on the results. The figures of this test are presented in Table 4.

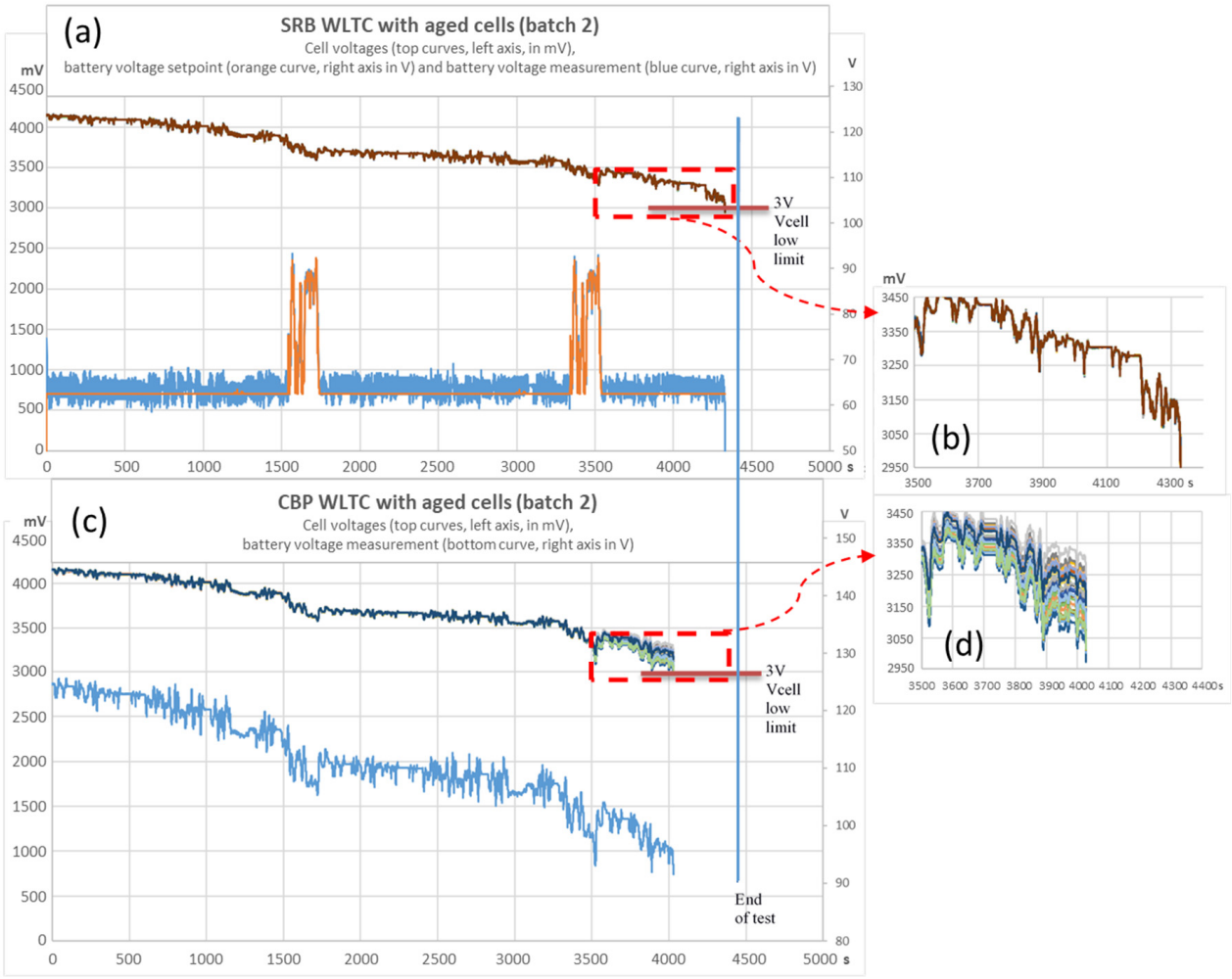

Figure 7. Driving profile with aged cells (batch 2): (**a**) SRB configuration results; (**b**) zoom on SRB configuration results; (**c**) CBP configuration results; (**d**) zoom on CBP configuration results. Cell voltages colors only to improve contrast.

Table 4. Figures of WLTC test with new cells (batch 2).

	CBP	**SRB**
Run time	4027 s	4329 s
Remaining energy at end of cycle	0 Wh	0 Wh
Cell balance at end of cycle	Δ = 220 mV	Δ < 5 mV
Discharged–charged energies	@4027 s: 1468 Wh	@4027 s: 1388 Wh @4329 s: 1436 Wh

4.3. Driving Profile with Second-Life Heterogeneous Cells (Batch 3)

The reparability of battery packs is becoming increasingly of interest to industry for the purpose of maintenance and optimizing system lifespan [39,40]. Heterogeneous cells in terms of capacity, and even different chemistries, can then constitute a reconditioned battery pack. To illustrate this, the operations of the CBP and the SRB are compared by conducting a driving profile with cells of heterogeneous capacities. Hence, a third batch

of 30 cells is made using a mix of new cells at 100% state of charge and new cells with a downgraded capacity, as shown in Figure 8. Eight cells in batch 1 are slightly discharged to present a reduced capacity, introducing a dispersion of 3.15% for batch 3. For accuracy, the lowered capacities are set before each test using a voltage threshold and a discharging current below C/10.

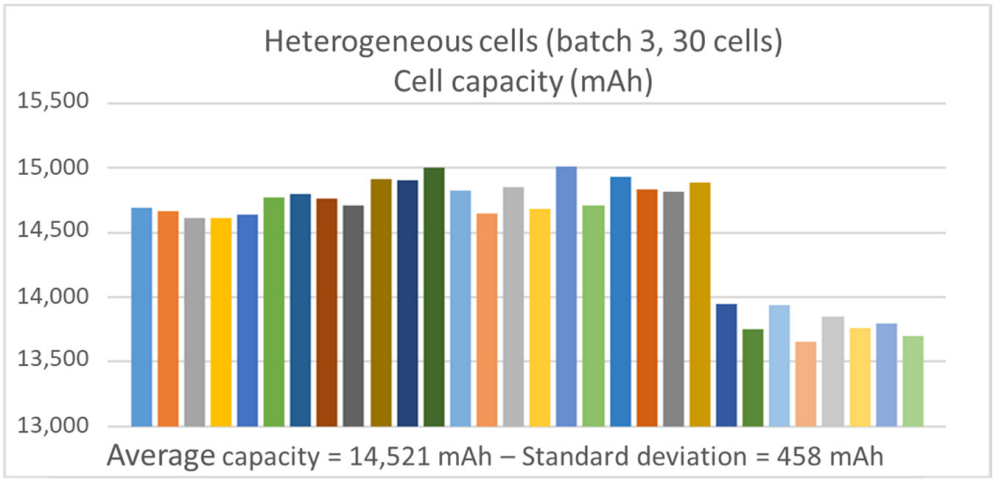

Figure 8. Heterogeneous capacity of cells constituting batch 3. Colors only to improve contrast.

The power profiles and the SRB set point profile are identical to those of the second batch discharge experiment, which had the same number of cells. The results of the driving profile applied to batch 3 are illustrated in Figure 9.

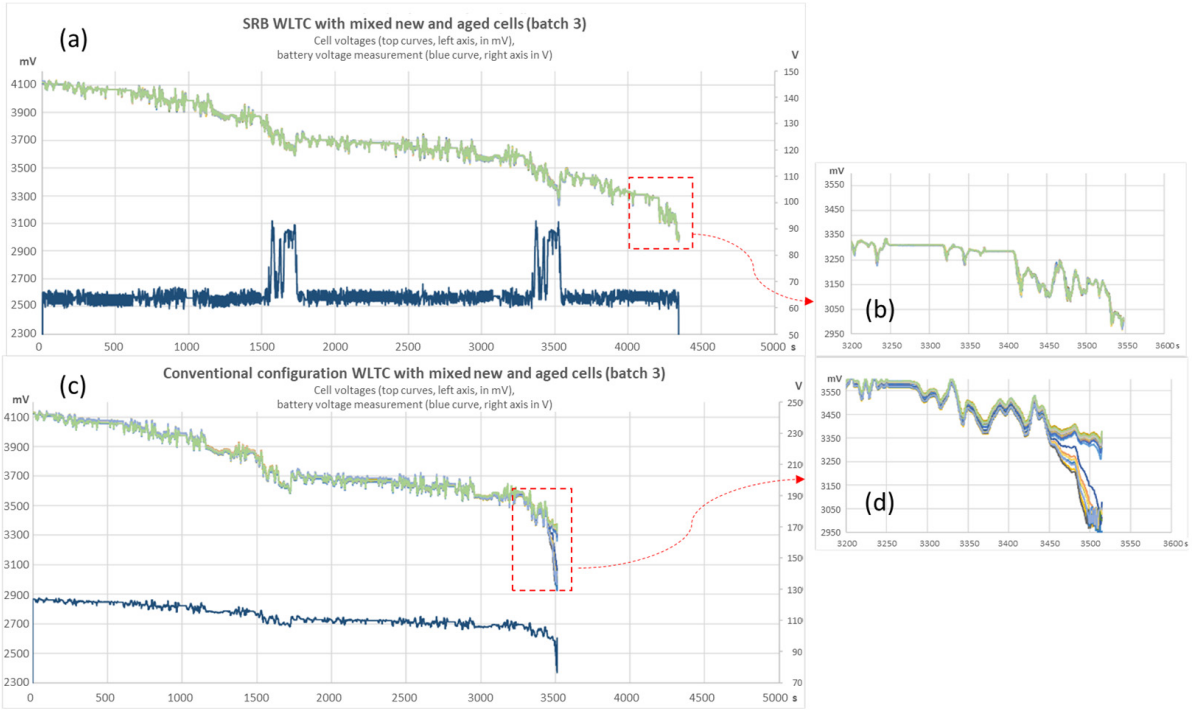

Figure 9. Driving profile with heterogeneous cells (batch 3): (**a**) SRB configuration results; (**b**) zoom on SRB configuration results; (**c**) CBP configuration results; (**d**) zoom on CBP configuration results. Cell voltages colors only to improve contrast.

In the CBP configuration, the weakest cell voltage drops before the others during the second high-power period of the WTLP cycle, causing the cycle to be halted at 3514 s, as shown in Figure 9c,d.

Figure 9a shows that the SRB is able to generate the output voltage corresponding to the voltage set point profile despite the use of a group of heterogeneous cells. The cells of the SRB are well balanced during the driving profile, while the battery voltage is controlled to maximize the inverter yield. The SRB allows weaker cells to be set aside while energy is extracted from all the other cells. Additionally, perfect balancing helps to avoid voltage drop due to high discharge current peaks, allowing the driving profile to continue. Hence, the system stops at 4347 s with perfectly balanced cells as shown in Figure 9b. The SRB consumes 5.3% less energy than the CBP for the same period of 3514 s. The figures of this test are presented in Table 5.

Table 5. Figures of WLTC test with cells from batch 3.

	CBP	**SRB**
Run time	3514 s	4347 s
Remaining energy at end of cycle	0 Wh	0 Wh
Cell balance at end of cycle	Δ = 428 mV	Δ = 21 mV
Discharged–charged energies	@3514 s: 1416 Wh	@3514 s: 1341.5 Wh @4347 s: 1437 Wh

4.4. Driving Profile with Cells from Real Battery Pack (Batch 4)

In industrial battery packs, cells with similar characteristics are assembled together to obtain the most homogenous batches possible during the manufacturing phase in order to maximize battery life [41]. In this test, the comparison is made using cells from a real 25,000 km industrial battery pack to show the benefits obtained from the slight dispersion of cells that can be found in real life. The driving profile is extended by repeating the same profile several times to match the increase in the battery capacity. The duration of the discharge process is calibrated to achieve a depth of discharge of approximately 10% of the battery's capacity for the two use cases where the discharged energies are compared. The profile is then repeated to fully discharge the battery in order to assess the energy remaining in each case.

The capacities of the fourth batch's cells used for this test are shown in Figure 10. The dispersion in capacity between cells in batch 4 is 0.37%. The capacity of the worst cell is approximately 91.67 A·h (98.57% of nominal capacity) with an average cell capacity of 92.29 A·h (99.23% of nominal capacity).

Test results are shown in Figure 11 with the SRB in the top part and the CBP in the bottom part. In both cases, the end of discharge is reached during a high-power phase. A state of charge of 10% is reached in 21,023 s in the CBP configuration, whereas the SRB configuration reaches 10% SOC in 21,869 s. In terms of energy, this leads to a reduced consumption of 4% when considering the energy consumed at 21,023 s for both configurations.

Regarding the total run time, the CBP configuration stops at 22,693 s, whereas the SRB configuration stops at 23,524 s, despite the fact that the SRB had to handle an additional power peak. In this context, the performance of the SRB dynamic balancing had no impact due to the very low imbalance of the cells from batch 4. Nevertheless, in terms of time duration, this leads to a gain of 3.66%, which is far from being insignificant considering the limited age of the battery pack. The figures of this test are presented in Table 6.

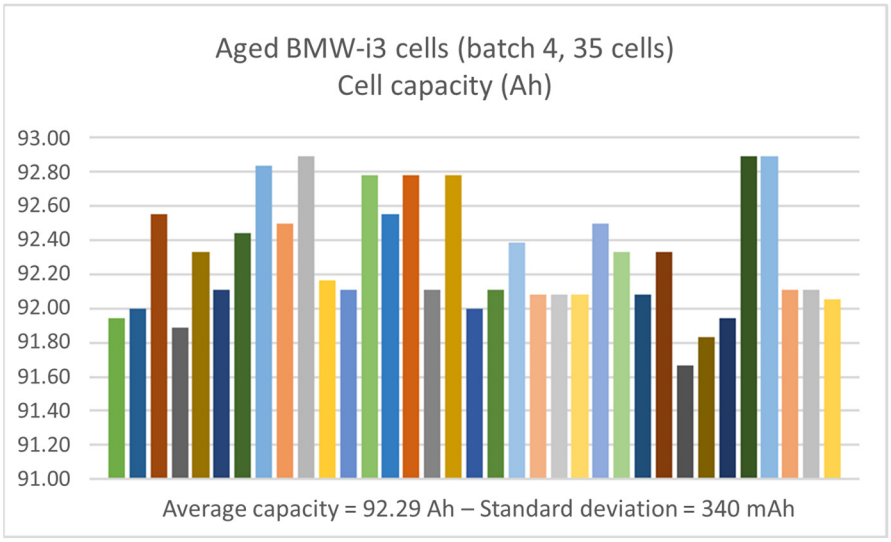

Figure 10. Capacity of cells from an aged BMW-i3 battery pack constituting batch 4. Colors only to improve contrast.

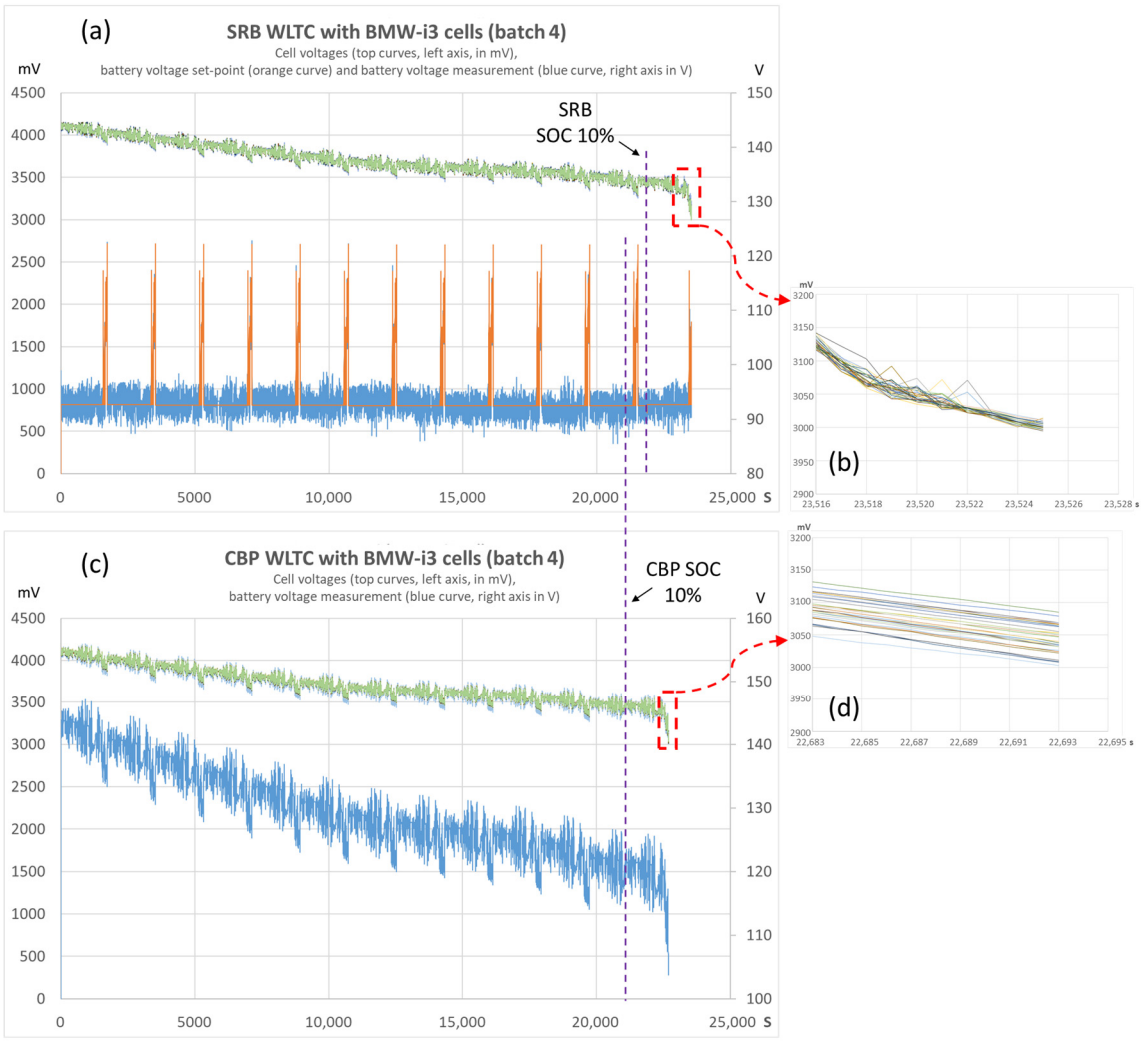

Figure 11. Driving profile with cells from a real BMW-i3 battery pack constituting batch 4: (**a**) SRB configuration results; (**b**) zoom on SRB configuration results; (**c**) CBP configuration results; (**d**) zoom on CBP configuration results. Cell voltages colors only to improve contrast.

Table 6. Figures of WLTC test with new cells (batch 4).

	CBP	SRB
Run time to 10%	21,023 s	21,869 s
Total run time	22,693 s	23,524 s
Remaining energy at end of cycle	989 Wh	976 Wh
Cell balance at end of cycle	Δ = 82 mV	Δ = 15 mV
Discharged–charged energies	@21,023 s: 10,192 Wh @22,693 s: 10,959 Wh	@21,023 s: 9783 W.h @21,869 s: 10,320 Wh @23,524 s: 11,076 Wh

4.5. Conclusion on Driving Profile

For each batch of cells tested, the conclusion is that the SRB manages to provide the dynamical output voltage corresponding to the voltage set point required to optimize the efficiency of the motor inverter. The fact that the observed difference in energy consumption corresponds to the difference predicted by the simulation shows that the imposed power profiles and the optimized voltage profile are consistent with the simulation presented in Section 2. In addition, good reproducibility is obtained with the different battery sizes.

Finally, the dynamic balancing capabilities of the SRB enable additional autonomy gains to be achieved by allowing the weakest cells to be set aside while energy is extracted from all the other cells. Perfectly balancing cells avoids voltage drop due to high discharge current peaks, enabling greater autonomy to be achieved with the driving profile.

5. Experimenting with Direct Charging of SRB on Electrical Grid

Removing the AC–DC inverters permits us to increase the charge yield [42]. To charge the Self-Reconfigurable Battery directly from the electrical grid without a charger, it is necessary to generate a perfectly synchronized voltage waveform. Furthermore, the voltage waveform of the electrical grid is never a perfect sinusoid; it has unpredictable distortions that must be taken into account when controlling the current exchanged with the battery. Due to the high control frequencies of the master controller, the SRB can produce an arbitrary voltage at its output. Hence, the output voltage of the SRB is directly adjusted in real time from the output of a charge current control loop that regulates the current exchanged with the electrical grid.

A Simulink algorithm is created to allow the SRB to be charged without a dedicated charger through a standard 16 A single-phase grid. The master controller contains a charge controller block based on this algorithm. This block receives as input the mean charge current set point and the instantaneous values of the grid voltage and the current exchanged. The output of this block is the number of cells to be connected in series, used to drive the output voltage in accordance with current regulation.

As the SRB developed for this study does not have the capacity to generate a negative voltage, a rectifier diode bridge is used to interface with the electrical grid. Filtering and safety elements are also added in series to the power circuit. The components used to connect the SRB to the power grid are illustrated in Figure 12, while the SRB architecture is illustrated in Figure 3.

At the beginning of the charging phase, the algorithm controls the SRB pack voltage until it matches the rectified grid voltage. When the signals are properly synchronized, a relay is closed to start charging. The start of SRB charging is shown in Figure 13 with the grid voltage (blue curve), the rectified grid voltage (green curve) and the charge current (pink curve). The test was carried out with a charging current of 3 A mean on a real electrical grid, so the sinusoidal curves are not perfect; nevertheless, the algorithm was able to perfectly match this voltage and its imperfections. Figure 14 shows a charge at 16 A. The shape of the current is always rectified and sinusoidal, regardless of the value of the current.

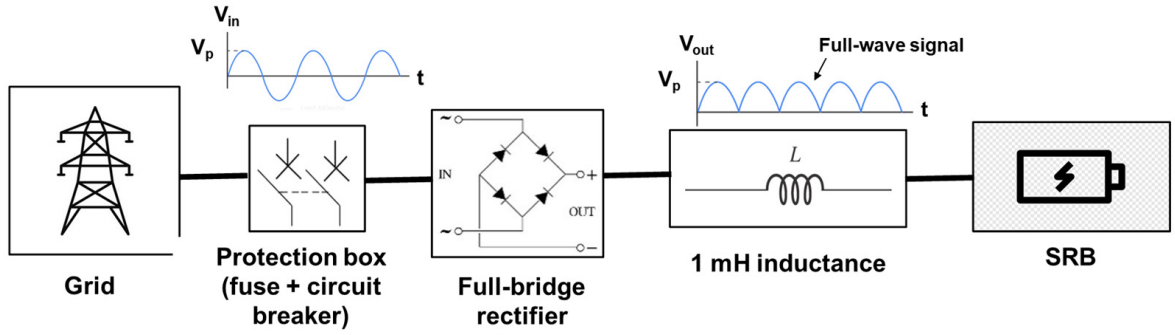

Figure 12. Elements between SRB and grid.

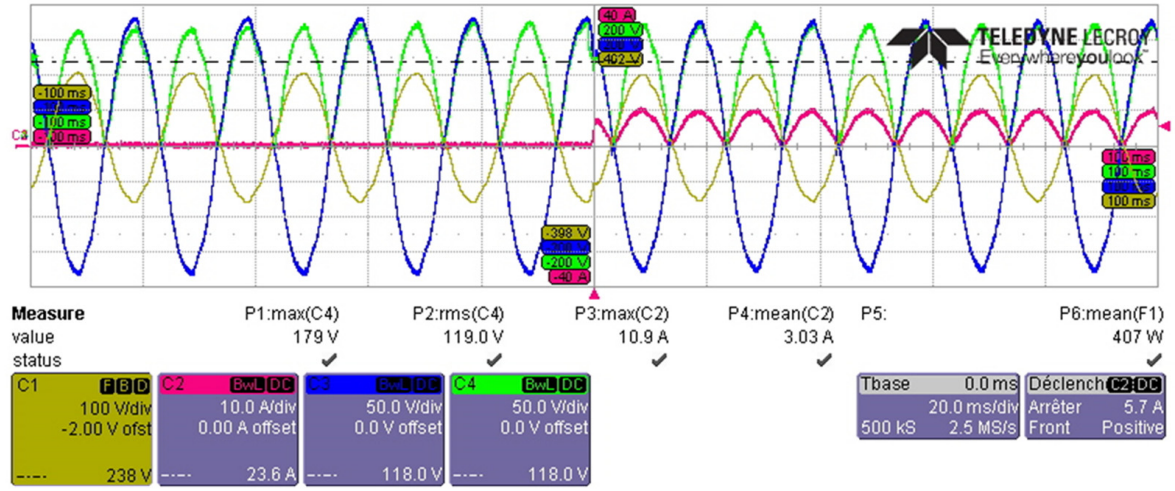

Figure 13. Start of SRB charging with electrical grid.

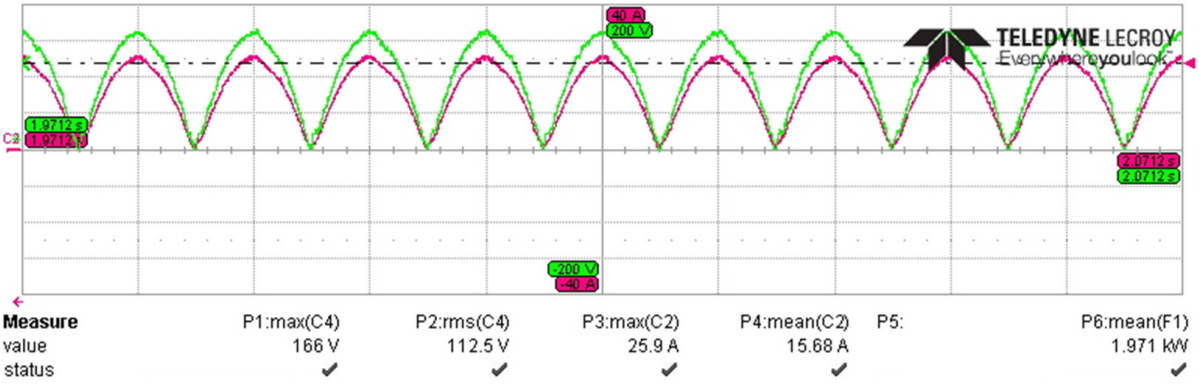

Figure 14. Rectified grid voltage (green) and charge current (pink) at 16 A mean.

6. Fast Charge Comparison

The objective of this test is to compare the behavior of the CBP and SRB during fast charging on a DC link. A first comparison is carried out with the same 12 modules using the batch 1 cells previously used for the WLTP tests. The first cell of each module is still permanently removed from the power path. A second comparison is carried out with eight modules from batch 4b, this time including the first stage of each module in the power path. Table 7 shows the batch characteristics used for each fast charge comparison.

Table 7. Batch characteristics used for fast charge comparison.

Cell Batch ID	Use Case	Cell Details	Nb of Cells	Nb of Modules	Nb of Cells Used for Comparison
1	Beginning of life	New NMC 14 Ah (CALB)	72	12	60
4b	Cells with a lifetime of around 25,000 real-life km	BMW-i3 NMC 94 Ah (SDI)	42	8	42

The charging current profile applied to the cells is adjusted according to the cell voltage, decreasing as the voltages approach end-of-charge conditions. To simplify control, the adjustment consists of three constant current amplitudes.

The Self-Reconfigurable Battery has the capability of individually bypassing cells at the end of their charge, whereas the Conventional Battery Pack must stop charging the whole system at the first cell in the end-of-charge state. Therefore, the criteria used to select the charging current level for each system must be different to take account of the differences in operation.

In the case of the CBP, the charging current level is affected by the voltage of the most charged cell, with different voltage thresholds to distinguish each level. However, a part of the cell voltage measured is related to the instantaneous current flowing through it due to its impedance. This voltage therefore decreases when the charging current is reduced. Hence, a hysteresis is added to the voltage thresholds to prevent a return to a higher charging current.

In the case of the SRB, only the highest voltage threshold 4.18 V is used to trigger a bypass of cells exceeding this value. The charging current level is then adjusted according to the number of cells remaining to be charged. The cells in bypass are put back into series when their voltage drops due to the relaxation effect. A hysteresis is applied to the voltage threshold used to reconnect the cells in series. This hysteresis is proportional to the amplitude of the charging current according to (1).

$$\text{Bypass to series Hysteresis [mV]} = \text{Current [A]}/1000 \quad (1)$$

The amplitude of the charge current for each level is adjusted between batch 1 and batch 4b to take account of the differences in terms of cell capacity. The cells in batch 1 are intended for power applications and accept a maximum continuous C-rate charge current of 10 C. Such a current is not recommended to preserve the health of the cells, but it is used in this study to illustrate the capabilities of the SRB electronics. It should be noted that in the case of batch 4b, the maximum current is limited by the current capacity of the test chamber. When the batch 4b cells are used, the experimental set-up has to change the test chamber, which reduces the capacity in terms of maximum current. As a result, the charge current rate is reduced for this batch, especially as the cells in batch 4b have a capacity 6.7 times greater than that of the cells in batch 1. This reduced charge rate enables the use of higher voltage thresholds for the CBP configuration. The fast charge conditions are summarized in Tables 8–10.

Table 8. Fast charge conditions for CBP using cells from batch 1.

CBP Condition	Batch 1 Charge Current (A)
VcellMax < 4.1 V	125 (8.9 C)
4 V < VcellMax < 4.15 V	24 (1.78 C)
4.14 V < VcellMax < 4.18 V	12 (0.86 C)

Table 9. Fast charge conditions for CBP using cells from batch 4b.

CBP Condition	Batch 4b Charge Current (A)
VcellMax < 4.15 V	90 (0.96 C)
4.05 V < VcellMax < 4.16 V	24 (0.25 C)
4.14 V < VcellMax < 4.18 V	12 (0.08 C)

Table 10. Fast charge conditions for SRB using cells from batch 1 and batch 4b.

SRB Condition	Batch 1 Charge Current (A)	Batch 4b Charge Current (A)
Series cell > 10 then 24 A	125 (8.9 C)	90 (0.96 C)
Series cell > 10 then 12 A	24 (1.78 C)	24 (0.25 C)
Series cell > 10 then stop	12 (0.86 C)	12 (0.08 C)

6.1. Comparison of Fast Charging with New Cells (Batch 1)

Figure 15 shows a comparison between the CPB and SRB during the fast charge phase with cells from batch 1.

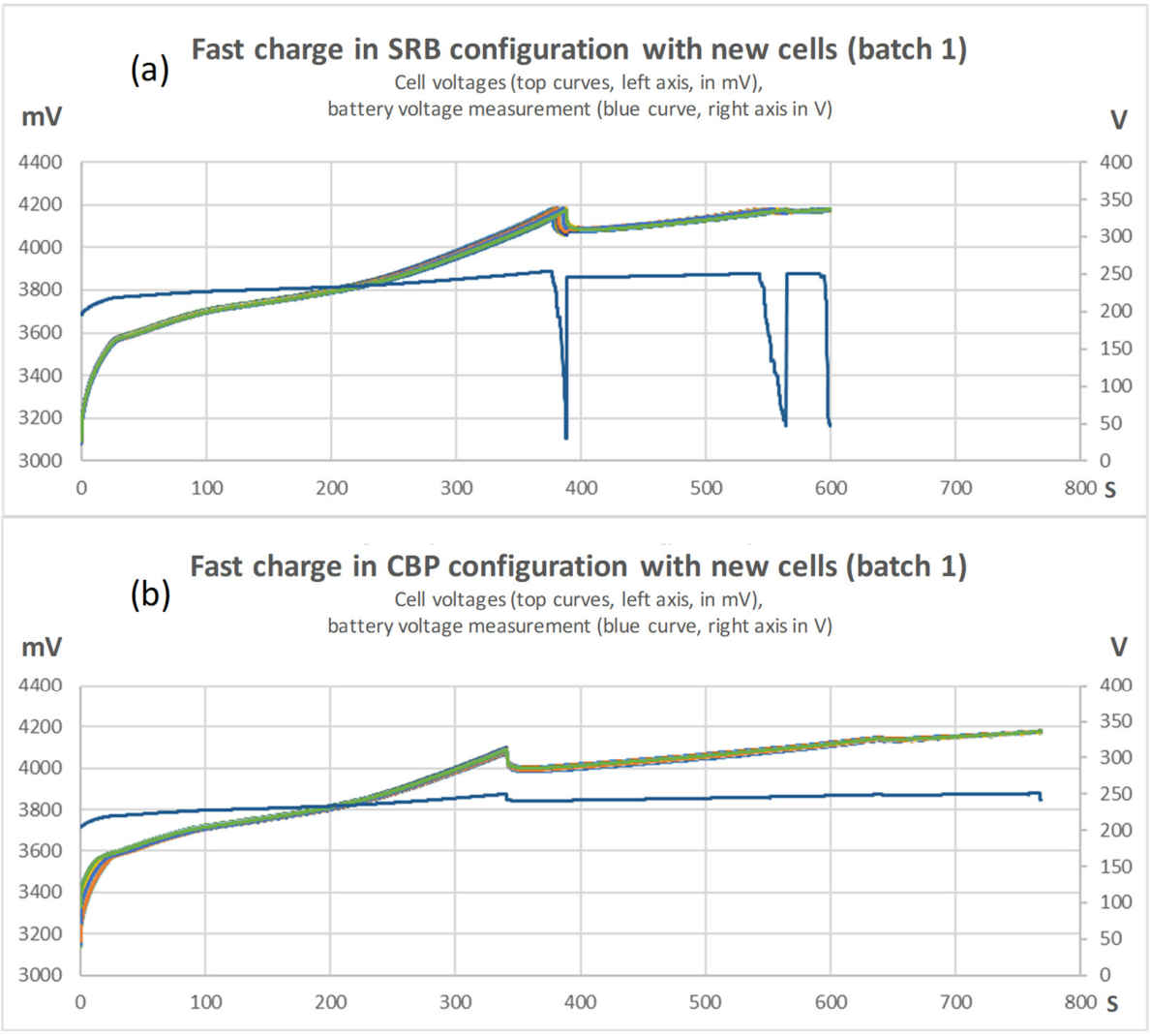

Figure 15. Comparison of charge for CBP and SRB configurations using cells from batch 1: (**a**) SRB configuration results; (**b**) CBP configuration results. Cell voltages colors only to improve contrast.

With the cells from batch 1, the state of charge 80% is reached before the first cell voltage threshold. Therefore, both the CBP and SRB reach this state of charge in around 332 s with a constant charging current of 125 A. The SRB is capable of bypassing a cell that reaches a voltage of 4.18 V and of reconnecting it in series when its voltage falls below a predefined threshold. In Figure 15a, the SRB voltage drops as cells are removed from the supply circuit when they reach this voltage threshold. When the number of cells in series falls below the 10-cell threshold, the charging current is reduced, which enables the SRB to return all cells to the power path, thus increasing the output voltage. One can note that the SRB takes advantage of the 80% to 100% state of charge interval to reach the full charge state in 22.8% less time than the CBP.

The total energy consumed by the charger is 3418 Wh for the SRB compared with 3342 Wh for the CBP, which represents a difference of 2.27%. This is due to the additional losses introduced by the series switches on the SRB. The figures of this test are presented in Table 11.

Table 11. Results of fast charging time for batch 1.

	CBP (s)	SRB (s)
SOC 20%	87	87
SOC 80%	332	334
Vcell max = 4.1 V	338	347
Vcell max = 4.15 V	502	366
SOC 100%	776	599

6.2. Comparison of Fast Charging with Cells from Real Battery Pack (Batch 4b)

Figure 16 shows a comparison between the CPB and SRB during the fast charge phase with cells from batch 4b. With the cells from batch 4b, the state of charge 80% is still reached before the first cell voltage threshold. Therefore, both the CBP and SRB reach this state of charge in 2908 s with a constant charging current of 90 A. It can be seen in Figure 16a that a longer time is needed for the SRB to fall below the 10-cell threshold, due to the reduced ratio between charging current and cell capacity. This longer time allows the discarded cells to be reconnected, resulting in a noisier SRB output voltage corresponding to alternating serial and bypass phases.

In this comparison, the SRB still takes advantage of the 80% to 100% state of charge interval to reach the full charge state 15.4% faster than the CBP. The total energy consumed by the charger is 17,645 Wh for the SRB compared with 17,007 Wh for the CBP. This represents a difference of 3.75%, this time including the first cells of each module from which energy is drawn to power the switching electronics. The figures of the fast charge comparison of batch 4b are presented in Table 12.

Table 12. Results of fast charging time for batch 4b.

	CBP (s)	SRB (s)
SOC 20%	727	727
SOC 80%	2908	2908
Vcell max = 4.15 V	2959	2978
Vcell max = 4.16 V	4069	3012
SOC 100%	6012	5087

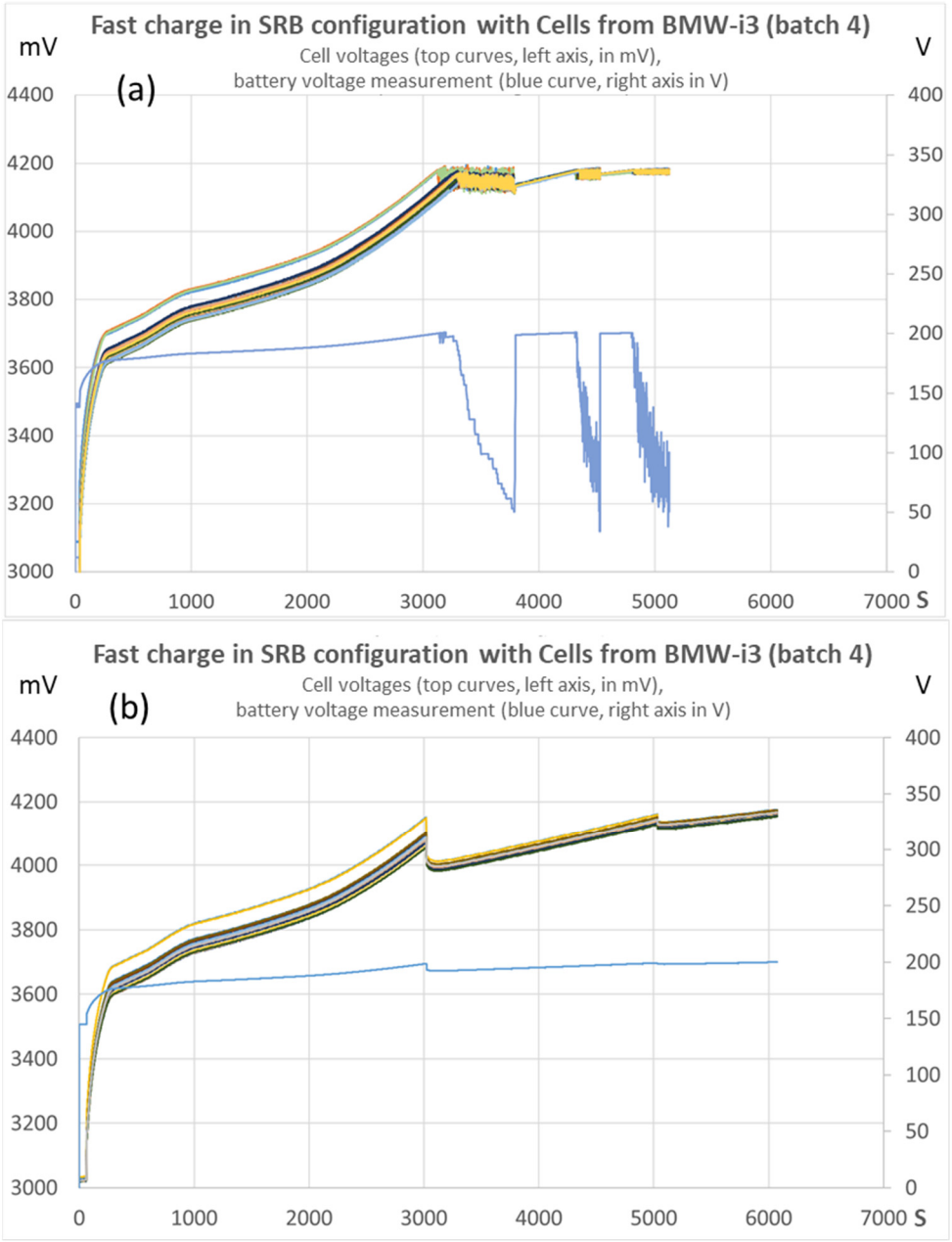

Figure 16. Comparison of charge for CBP and SRB configurations using cells from batch 4b: (**a**) SRB configuration results; (**b**) CBP configuration results. Cell voltages colors only to improve contrast.

7. Discussion

The experimental system is not far from being able to be integrated into a demonstrator vehicle, given the level of maturity above TRL 4 achieved by the developments initiated since 2012 at the CEA [43], as well as the size of the demonstrator in terms of on-board battery as well as power, current and voltage capacity.

The experimental validation of the results obtained by simulation demonstrates that it is possible to simulate the behavior of a real SRB device at vehicle scale with a good level of representativeness. This demonstration is especially important as it was carried out using the models and simulation tools developed by Vitesco for its industrial development processes.

With regard to the results obtained with the different batches of cells, it can be seen that the disparities between the cells do not affect the ability of the experimental SRB to generate the voltage profile required to optimize the inverter's efficiency.

The results also show that the impact of an SRB's balancing performance depends on the unbalanced characteristics of the cells and the power rating used at the end of the discharge. It can be seen that the higher the power demand at the end of discharge, the greater the impact on the SRB's balancing capacity. In this respect, it is important to note that perfectly balancing cell voltage before a power peak is not necessarily sufficient. Managing the voltage drops of the cells with the highest impedance during the power peak is also significant. In the case of this study, the proposed SRB system is able to replace in real time an active cell reaching its end-of-discharge voltage threshold. The swap with an inactive cell of any local controller is performed in a time interval of less than a few tens of microseconds, so that no disturbance of the output voltage occurs. In addition to the gains in autonomy presented in this study, we can therefore expect to see interesting gains in terms of power availability.

With regard to fast charging on a DC source, the main contribution of SRB systems is made from the time at which the conventional system reaches the first conditions requiring a drop in charging current. In this study, the conditions are voltage conditions, but they could also be over-temperature conditions in certain contexts as seen in the simulation or even conditions related to model-based parameters that the state of the art is beginning to use to optimize fast charging in conventional systems [44]. In this area, SRBs could gain an advantage from the prospect of improved cell parameter identification capabilities [45–47].

Despite all the advantages mentioned above, the adoption of reconfigurable batteries in the industrial sector is currently limited to start-up companies such as SwitchESS, with which the CEA has collaborated [48], or Bavertis [49]. The integration of reconfigurable batteries involves concentrating responsibility for a range of functions, such as the battery, the BMS, the charger and even the motor inverter. For Tier 1 manufacturers, this represents an important challenge, both economically and technically. Recently, the industry has taken a close interest in this technology, as shown by the interest expressed by Vitesco [50] and Stellantis [51].

8. Conclusions

This paper reports the results of simulation and experimentation of the advanced capabilities of a Self-Reconfigurable Battery, including battery output voltage control, active balancing during operation, AC grid charging without an inverter and fast DC charging. The performance of the SRB as a DC–DC power source is compared to that of a Conventional Battery Pack, revealing improved efficiency and faster charge rates. Specifically, the SRB increased the driving range by 6% and reduced charging time by 22%. In addition, the experimental results demonstrate the SRB's ability to operate heterogeneous cells correctly and extend battery life by reproducing the aging observed in real automotive batteries. It also demonstrates the capability of using unsorted cells or heterogeneous cells for second life.

To extend this study, given that the SRB introduces many more electronic components than the CBP, elements other than performance need to be taken into account to make a fair comparison between the two solutions, such as cost, reliability and safety.

As far as the cost aspect is concerned, estimating the economic benefit of reconfigurable batteries is complex because it has to integrate the benefits at the level of the overall system to be relevant. For example, improving the energy efficiency of the powertrain as a whole can reduce the cost of the battery for an equivalent range. Additionally, this improvement can also reduce the amount of CO_2 equivalent consumed, which is a very important cost criterion for manufacturers because of the regulations introduced in recent years. The cells are also less susceptible to aging, which extends the life of the pack and therefore saves the consumer a certain amount of money. Still on the economic aspect, the SRB's ability to integrate heterogeneous cells opens the way to the use of batteries that could be less expensive to produce because they would be less constrained in terms of homogeneity, or even could be from second life. In all the cases mentioned, dedicated detailed studies would be required to estimate the savings made.

From a reliability point of view, the large number of components used for switching raises questions, especially when SRBs are paradoxically highlighted for their ability to improve battery reliability by isolating faulty cells. However, SRBs have a certain potential because, although they use a large number of components, the mature manufacturing process of MOSFET and limited voltage range required make them more reliable than the increasingly sophisticated power components such as SIC and GAN switches used in power converters, even more so as the voltage levels of battery packs are becoming higher and higher to meet the constraints of rapid charging. The number of components used must therefore be considered in light of the Mean Time Between Failures (MTBF), by means of a rigorous analysis of the system's fault tree.

From the point of view of software constraints, the greater the complexity of the code, the more difficult and costly it is to ensure. The use of a distributed system such as the one presented in this study makes it possible to partition the software functions. In this way, the role of the software corresponding to the local controllers can be limited to ensuring the translation of the serial/bypass commands received from the central controller into local switch control with the appropriate transitions. In this way, it is possible to simplify the software used by the local controllers as much as possible in order to guarantee a satisfactory level of reliability and safety. This allows for mitigating the level of criticality applied to the central node software.

This project is a unique opportunity to work on these points, and the initial analysis shows that an SRB designed to automotive standards in a robust and safe manner could be a competitive solution if the powertrain is considered as a whole, including throughout its lifetime. Overall, this study highlights the impressive capabilities of an SRB and its potential for use in a variety of applications.

Author Contributions: Conceptualization, R.T., N.L., J.L., S.B., Y.L. and L.C.; methodology, R.T., N.L., J.L., S.B. and Y.L.; software, R.T., S.B. and L.C.; validation R.T., N.L., J.L., S.B., Y.L. and L.C.; writing—original draft preparation, R.T., N.L., J.L. and S.B.; writing—review and editing, R.T., N.L., J.L. and S.B.; supervision, N.L. and S.B.; project administration, N.L. and S.B. All authors have read and agreed to the published version of the manuscript.

Funding: This research has benefited from the support of the Automotive and Mobility Research Steering Committee (CORAM) funded by BPIFRANCE.

Data Availability Statement: The raw data supporting the conclusions of this article will be made available by the authors on request.

Acknowledgments: This work has benefited from technical support from A. Bouche-Pillon and M. Bey, for the use of the test chamber equipment, the generating of power cycles from the calculated power exchange files and the data logging.

Conflicts of Interest: Nicolas Léto, Jérome Lachaize are employees of Vitesco Technologies. The paper reflects the views of the scientists, and not the company.

Abbreviations

Symbols	Descriptions
BEV	Battery Electric Vehicle
CBP	Conventional Battery Pack
CEA	French Alternative Energies and Atomic Energy Commission
EVS36	36th Electrical Vehicle Symposium
SOC	state of charge
SOH	State Of Health
SRB	Self-Reconfigurable Battery
NMC	Nickel Manganese Cobalt oxides
WLTP	Worldwide harmonized Light vehicles Test Procedure
TRL	Technology Readiness Level
MTBF	Mean Time Between Failures

References

1. Komsiyska, L.; Buchberger, T.; Diehl, S.; Ehrensberger, M.; Hanzl, C.; Hartmann, C.; Hölzle, M.; Kleiner, J.; Lewerenz, M.; Liebhart, B.; et al. Critical Review of Intelligent Battery Systems: Challenges, Implementation, and Potential for Electric Vehicles. *Energies* **2021**, *14*, 5989. [CrossRef]
2. Thomas, R.; Lehmann, F.; Blatter, J.; Despesse, G.; Heiries, V. Performance Analysis of a Novel High Frequency Self-Reconfigurable Battery. *World Electr. Veh. J.* **2021**, *12*, 10. [CrossRef]
3. Baccari, S.; Tipaldi, M.; Mariani, V. Deep Reinforcement Learning for Cell Balancing in Electric Vehicles with Dynamic Reconfigurable Batteries. *IEEE Trans. Intell. Veh.* **2024**, 1–12. [CrossRef]
4. Wiedenmann, A.; Buberger, J.; Högerl, T.; Grupp, W.; Hohenegger, M.; Kuder, M.; Weyh, T.; Neve, A. Proactive Balancing for Reconfigurable Battery Systems with Automated Efficiency Analysis. In Proceedings of the 2023 International Conference on Smart Energy Systems and Technologies (SEST), Mugla, Turkiye, 4–6 September 2023. [CrossRef]
5. Lee, S.; Noh, G.; Ha, J.-I. Reconfigurable Power Circuits to Series or Parallel for Energy-Balanced Multicell Battery Pack. *IEEE Trans. Ind. Electron.* **2023**, *70*, 3641–3651. [CrossRef]
6. Li, Y.; Yin, P.; Chen, J. Active Equalization of Lithium-Ion Battery Based on Reconfigurable Topology. *Appl. Sci.* **2023**, *13*, 1154. [CrossRef]
7. Karnehm, D.; Bliemetsrieder, W.; Pohlmann, S.; Neve, A. Controlling Algorithm of Reconfigurable Battery for State of Charge Balancing Using Amortized Q-Learning. *Batteries* **2024**, *10*, 131. [CrossRef]
8. Lamprecht, A.; Narayanaswamy, S.; Steinhorst, S. Improving Fast Charging Efficiency of Reconfigurable Battery Packs. In Proceedings of the 2018 Design, Automation & Test in Europe Conference & Exhibition (DATE), Dresden, Germany, 19–23 March 2018. [CrossRef]
9. Balachandran, A.; Jonsson, T.; Eriksson, L. DC Charging Capabilities of Battery-Integrated Modular Multilevel Converters Based on Maximum Tractive Power. *Electricity* **2023**, *4*, 62–77. [CrossRef]
10. Buberger, J.; Hohenegger, M.; Estaller, J.; Wiedenmann, A.; Grupp, W.; Bliemetsrieder, W.; Kuder, M.; Lesnicar, A.; Weyh, T. Bidirectional Charging for BEVs with Reconfigurable Battery Systems via a Grid-Parallel Proportional-Resonant Controller. *Electricity* **2023**, *4*, 171–184. [CrossRef]
11. Prasad, R.; Namuduri, C.; Gopalakrishnan, S. On-Demand Battery Reconfiguration for 800V DC Fast Charging in Electric Vehicles. In Proceedings of the 2023 IEEE Energy Conversion Congress and Exposition (ECCE), Nashville, TN, USA, 29 October–2 November 2023. [CrossRef]
12. Sorokina, N.; Estaller, J.; Kersten, A.; Buberger, J.; Kuder, M.; Thiringer, T.; Eckerle, R.; Weyh, T. Inverter and Battery Drive Cycle Efficiency Comparisons of Multilevel and Two-Level Traction Inverters for Battery Electric Vehicles. In Proceedings of the 2021 IEEE International Conference on Environment and Electrical Engineering and 2021 IEEE Industrial and Commercial Power Systems Europe (EEEIC/I&CPS Europe), Bari, Italy, 7–10 September 2021. [CrossRef]
13. Xu, Y.; Kersten, A.; Ingelström, P.; Amirpour, S.; Klacar, S.; Sedarsky, D. Comparative Study of Efficiency Improvement with Adjustable DC-Link Voltage Powertrain Using DC-DC Converter and Quasi-Z-Source Inverter. In Proceedings of the 2023 IEEE Transportation Electrification Conference and Expo, Asia-Pacific (ITEC Asia-Pacific), Chiang Mai, Thailand, 28 November–1 December 2023. [CrossRef]
14. Li, Z.; Yang, A.; Chen, G.; Tashakor, N.; Zeng, Z.; Peterchev, A.V.; Goetz, S.M. A Rapidly Reconfigurable DC Battery for Increasing Flexibility and Efficiency of Electric Vehicle Drive Trains. *IEEE Trans. Transp. Electrif.* **2024**, 1. [CrossRef]
15. Blatter, J.; Heiries, V.; Thomas, R.; Despesse, G. Optimal Lifetime Management Strategy for Self-Reconfigurable Batteries. In Proceedings of the 2022 IEEE 95th Vehicular Technology Conference: (VTC2022-Spring), Helsinki, Finland, 19–22 June 2022. [CrossRef]
16. Kacetl, T.; Kacetl, J.; Tashakor, N.; Goetz, S. Ageing Mitigation and Loss Control in Reconfigurable Batteries in Series-Level Setups. In Proceedings of the EPE 2022 ECCE Europe, Hanover, Germany, 5 September 2022.
17. Škegro, A.; Zou, C.; Wik, T. Analysis of Potential Lifetime Extension through Dynamic Battery Reconfiguration. In Proceedings of the 2023 25th European Conference on Power Electronics and Applications (EPE'23 ECCE Europe), Aalborg, Denmark, 4–8 September 2023; pp. 1–11. [CrossRef]
18. Kuder, M.; Schneider, J.; Kersten, A.; Thiringer, T.; Eckerle, R.; Weyh, T. Battery Modular Multilevel Management (BM3) Converter Applied at Battery Cell Level for Electric Vehicles and Energy Storages. In Proceedings of the PCIM Europe Digital Days 2020; International Exhibition and Conference for Power Electronics, Intelligent Motion, Renewable Energy and Energy Management, Nuremburg, Germany, 7–8 July 2020; pp. 1–8.
19. D'Arco, S.; Quraan, M.; Tricoli, P.; Piegari, L. Low frequency operation of Modular Multilevel Converters with embedded battery cells for traction drives. In Proceedings of the 2016 International Symposium on Power Electronics, Electrical Drives, Automation and Motion, SPEEDAM, Anacapri, Italy, 22–24 June 2016; pp. 1375–1382. [CrossRef]
20. Davis, A.; Salameh, Z.M.; Eaves, S.S. Comparison of a synergetic battery pack drive system to a pulse width modulated AC induction motor drive for an electric vehicle. *IEEE Trans. Energy Convers.* **1999**, *14*, 245–250. [CrossRef]
21. Sorokina, N.; Högerl, T.; Wolfgang, B.; Hein, L.; Weyh, T.; Kuder, M. Investigation of Reconfigurable Battery Efficiency for an Application in an Electrical Sailplane. In Proceedings of the 2023 25th European Conference on Power Electronics and Applications (EPE'23 ECCE Europe), Aalborg, Denmark, 4–8 September 2023; pp. 1–8. [CrossRef]

22. Davis, A.; Salameh, Z.M.; Eaves, S.S. Evaluation of lithium-ion synergetic battery pack as battery charger. *IEEE Trans. Energy Convers.* **1999**, *14*, 830–835. [CrossRef]
23. Leite, R.S.; Afonso, J.L.; Monteiro, V. A Novel Multilevel Bidirectional Topology for On-Board EV Battery Chargers in Smart Grids. *Energies* **2018**, *11*, 3453. [CrossRef]
24. Vemuganti, H.P.; Sreenivasarao, D.; Ganjikunta, S.K.; Suryawanshi, H.M.; Abu-Rub, H. A Survey on Reduced Switch Count Multilevel Inverters. *IEEE Open J. Ind. Electron. Soc.* **2021**, *2*, 80–111. [CrossRef]
25. Schmid, M.; Gebauer, E.; Endisch, C. Structural Analysis in Reconfigurable Battery Systems for Active Fault Diagnosis. *IEEE Trans. Power Electron.* **2021**, *36*, 8672–8684. [CrossRef]
26. Xu, H.; Cheng, L.; Xu, S.; Liu, C.; Paizulamu, D. Operating Performance Evaluation and Improvement Method of Reconfigurable Battery Energy Storage System. In Proceedings of the 2022 12th International Conference on Power and Energy Systems (ICPES), Guangzhou, China, 23–25 December 2022. [CrossRef]
27. Bayati, M.; Tashakor, N.; Farahmandrad, M.; Abkenar, P.P.; Goetz, S. Fault-Tolerant Electric Vehicle Drivetrain with Reconfigurable Battery and Multiphase Machine. In Proceedings of the 2023 IEEE 2nd Industrial Electronics Society Annual On-Line Conference (ONCON), Online, 8–10 December 2023. [CrossRef]
28. Thomas, R.; Despesse, G.; Bacquet, S.; Fernandez, E.; Lopez, Y.; Ramahefa-Andry, P.; Cassarino, L. A High Frequency Self-Reconfigurable Battery for Arbitrary Waveform Generation. *World Electr. Veh. J.* **2021**, *12*, 8. [CrossRef]
29. Braco, E.; San Martín, I.; Sanchis, P.; Ursúa, A. Characterization and Capacity Dispersion of Lithium-Ion Second-Life Batteries from Electric Vehicles. In Proceedings of the 2019 IEEE International Conference on Environment and Electrical Engineering and 2019 IEEE Industrial and Commercial Power Systems Europe (EEEIC/I&CPS Europe), Genova, Italy, 11–14 June 2019. [CrossRef]
30. Bacquet, S.; Léto, N.; Lachaize, J.; Thomas, R.; Lopez, Y.; Cassarino, L. Simulation and testing of self reconfigurable battery advanced functions for automotive application. In Proceedings of the 36th International Electric Vehicle Symposium and Exhibition (EVS36), Sacramento, CA, USA, 11–14 June 2023.
31. Ayad, A.; Léto, N.; Schweizer Berberich, N.; Bornschlegel, S.; Lachaize, J.; Hevele, N.; Brockerhoff, P.; Lyubar, A. Active and Power Balancing Techniques: More Range and Longer Cell Lifetime in Electric Vehicles. In Proceedings of the 35th International Electric Vehicle Symposium and Exhibition (EVS35), Oslo, Norway, 11–15 June 2022.
32. Gnann, T.; Funke, S.; Jakobsson, N.; Plötz, P.; Sprei, F.; Bennehag, A. Fast charging infrastructure for electric vehicles: Today's situation and future needs. *Transp. Res. Part D Transp. Environ.* **2018**, *62*, 314–329. [CrossRef]
33. Ci, S.; Lin, N.; Wu, D. Reconfigurable Battery Techniques and Systems: A Survey. *IEEE Access* **2016**, *4*, 1175–1189. [CrossRef]
34. Kirkaldy, N.; Samieian, M.A.; Offer, G.J.; Marinescu, M.; Patel, Y. Lithium-ion battery degradation: Comprehensive cycle ageing data and analysis for commercial 21700 cells. *J. Power Sources* **2024**, *603*, 234185. [CrossRef]
35. Beck, D.; Dechent, P.; Junker, M.; Sauer, D.U.; Dubarry, M. Inhomogeneities and Cell-to-Cell Variations in Lithium-Ion Batteries, a Review. *Energies* **2021**, *14*, 3276. [CrossRef]
36. Naguib, M.; Kollmeyer, P.; Emadi, A. Lithium-Ion Battery Pack Robust State of Charge Estimation, Cell Inconsistency, and Balancing: Review. *IEEE Access* **2021**, *9*, 50570–50582. [CrossRef]
37. Schindler, M.; Sturm, J.; Ludwig, S.; Schmitt, J.; Jossen, A. Evolution of initial cell-to-cell variations during a three-year production cycle. *eTransportation* **2021**, *8*, 100102. [CrossRef]
38. Schuster, S.F.; Brand, M.J.; Berg, P.; Gleissenberger, M.; Jossen, A. Lithium-ion cell-to-cell variation during battery electric vehicle operation. *J. Power Sources* **2015**, *297*, 242–251. [CrossRef]
39. Martinez-Laserna, E.; Sarasketa-Zabala, E.; Stroe, D.I.; Swierczynski, M.; Warnecke, A.; Timmermans, J.M.; Goutam, S.; Rodriguez, P. Evaluation of lithium-ion battery second life performance and degradation. In Proceedings of the 2016 IEEE Energy Conversion Congress and Exposition (ECCE), Milwaukee, WI, USA, 18–22 September 2016; pp. 1–7. [CrossRef]
40. Hossain, E.; Murtaugh, D.; Mody, J.; Faruque, H.M.R.; Haque Sunny, M.S.; Mohammad, N. A Comprehensive Review on Second-Life Batteries: Current State, Manufacturing Considerations, Applications, Impacts, Barriers & Potential Solutions, Business Strategies, and Policies. *IEEE Access* **2019**, *7*, 73215–73252. [CrossRef]
41. Baumhöfer, T.; Brühl, M.; Rothgang, S.; Sauer, D.U. Production caused variation in capacity aging trend and correlation to initial cell performance. *J. Power Sources* **2014**, *247*, 332–338. [CrossRef]
42. Genovese, A.; Ortenzi, F.; Villante, C. On the Energy Efficiency of Quick DC Vehicle Battery Charging. *World Electr. Veh. J.* **2015**, *7*, 570–576. [CrossRef]
43. Despesse, G.; Sanjuan, S.L.; Gery, S. Battery Monitoring System Using Switching Battery Cells. In Proceedings of the RITF 2012—Research & Innovation for Transport Systems of the Future, Paris, France, 12–15 November 2012; pp. 12–15, hal-01681862.
44. Li, Y.; Vilathgamuwa, D.M.; Wikner, E.; Wei, Z.; Zhang, X.; Thiringer, T.; Wik, T.; Zou, C. Electrochemical Model-Based Fast Charging: Physical Constraint-Triggered PI Control. *IEEE Trans. Energy Convers.* **2021**, *36*, 3208–3220. [CrossRef]
45. Kersten, A.; Kuder, M.; Han, W.; Thiringer, T.; Lesnicar, A.; Weyh, T.; Eckerle, R. Online and On-Board Battery Impedance Estimation of Battery Cells, Modules or Packs in a Reconfigurable Battery System or Multilevel Inverter. In Proceedings of the IECON 2020 the 46th Annual Conference of the IEEE Industrial Electronics Society, Singapore, 18–21 October 2020. [CrossRef]
46. Schneider, D.; Liebhart, B.; Endisch, C. Active State and Parameter Estimation as Part of Intelligent Battery Systems. *J. Energy Storage* **2021**, *39*, 102638. [CrossRef]
47. Theiler, M.; Schneider, D.; Endisch, C. Experimental Investigation of State and Parameter Estimation within Reconfigurable Battery Systems. *Batteries* **2023**, *9*, 145. [CrossRef]

48. SwitchESS Cell-Wise Driving. Available online: https://switchess.com (accessed on 17 May 2024).
49. Bavertis. Available online: https://bavertis.com (accessed on 17 May 2024).
50. Concentrated Competence in Battery Management: Vitesco Technologies France Cooperates with CEA. Available online: https://www.leti-cea.com/cea-tech/leti/english/Pages/What's-On/Press%20release/Concentrated-competence-in-battery-management-Vitesco-Technologies-France-cooperates-with-CEA.aspx (accessed on 17 May 2024).
51. IBIS: Stellantis and Saft Reveal a Smarter, More Efficient Battery for Autos and Stationary Power. Available online: https://www.stellantis.com/en/news/press-releases/2023/july/ibis-stellantis-and-saft-reveal-a-smarter-more-efficient-battery-for-autos-and-stationary-power?adobe_mc_ref= (accessed on 17 May 2024).

Disclaimer/Publisher's Note: The statements, opinions and data contained in all publications are solely those of the individual author(s) and contributor(s) and not of MDPI and/or the editor(s). MDPI and/or the editor(s) disclaim responsibility for any injury to people or property resulting from any ideas, methods, instructions or products referred to in the content.